

Multifunctional Altermagnet with Large Out-of-Plane Piezoelectric Response in Janus V_2AsBrO Monolayer

Qiuyue Ma, Busheng Wang, Guochun Yang, and Yong Liu*

State Key Laboratory of Metastable Materials Science and Technology

& Hebei Key Laboratory of Microstructural Material Physics,

School of Science, Yanshan University, Qinhuangdao 066004, China

Abstract

Altermagnetism has emerged as a third fundamental category of collinear magnetism, characterized by spin-splitting in symmetry-compensated collinear antiferromagnets, opening new frontiers in spintronics and condensed matter physics. Here, based on first-principles calculations, we propose a novel altermagnetic semiconductor, the asymmetric Janus V_2AsBrO monolayer, which exhibits a magnetic easy axis favoring the out-of-plane direction and a Néel temperature (T_N) exceeding room temperature. The system exhibits a strain-tunable piezovally effect, generating valley polarization under uniaxial strain. Notably, hole doping under uniaxial strain generates a net magnetization (M) through a piezomagnetic mechanism. Additionally, the broken inversion symmetry endows the monolayer with a substantial out-of-plane piezoelectric coefficient d_{31} (2.19 pm/V), presenting broad prospects for the development and design of novel piezoelectric devices. Our findings provide a promising candidate material for the advancement of 2D multifunctional devices in nanoelectronics, spintronics, valleytronics, and piezoelectrics.

* yongliu@ysu.edu.cn

I. INTRODUCTION

Two-dimensional (2D) antiferromagnetic (AFM) materials are highly promising candidates for next-generation devices and technologies due to their robustness against magnetic disturbances, ultrafast dynamics, absence of stray fields, higher speed operation, and lower-energy consumption [1–3]. However, the counterpart spin degeneracy in real and reciprocal space of conventional antiferromagnets hinders the realization of spin-polarized currents. Recently, a new type of collinear magnetism called ‘altermagnetism’ has garnered significant attention in the fields of spintronics and magnetic materials research [4–7]. Altermagnetic materials exhibit spin splitting without relying on relativistic spin-orbit coupling (SOC) by breaking \mathcal{PT} symmetry, in which \mathcal{P} is spatial inversion symmetry and \mathcal{T} is time-reversal symmetry [8–11], and maintaining AFM order with no net magnetic moment. The novel physical phenomena observed in altermagnets, such as giant and tunneling magnetoresistance [12, 13], spin current generation [14, 15], anomalous Hall effect [16], and suppressed Kondo effect [17], are prompting the development of multifunctional electronic devices.

Manipulating energy valleys in the conduction/valence bands to encode, transfer, and store information is characterized as valleytronics [18–21]. In recent years, various 2D materials, such as graphene and the $2H$ -phase transition metal dichalcogenides (TMDs) MX_2 , have been identified as promising candidates for valleytronic applications. In these materials, the K and K' valleys are related through \mathcal{T} symmetry. However, the valleys in altermagnetic materials are comprised of spin-polarized valleys related by a crystal symmetry instead of the \mathcal{T} symmetry. Ma et al. defined these as crystal symmetry-related valleys (\mathcal{C} -paired valleys), which, compared to time-reversal symmetry-related valleys (\mathcal{T} -paired valleys), exhibit more intriguing properties in terms of valley polarization [22]. Therefore, applying uniaxial strain to break the crystal symmetry can induce the valley splitting in altermagnetic materials, upon finite doping can further induce a net magnetization (M) [23].

Recent advances in multifunctional 2D piezoelectric materials have spurred extensive experimental and theoretical investigations, positioning them as promising platforms for next-generation multifunctional electronics. [24–30]. The piezoelectric effect occurs in semiconductors with non-centrosymmetric crystal structures [31, 32]. In 2D altermagnetic materials, such as CrO [33], $\text{V}_2\text{Se}_2\text{O}$ [22], $\text{Fe}_2\text{Se}_2\text{O}$ [34], and $\text{Cr}_2\text{Te}_2\text{O}$ [35] have inversion symmetry, leading to missing piezoelectricity. Searching for 2D piezoelectric altermagnetism (PAM) is

both significant and challenging. A substantial out-of-plane piezoelectric response is highly desirable for practical applications, as it ensures compatibility with current bottom/top gate technologies. Therefore, altermagnetic materials with a significant out-of-plane piezoelectric response are promising candidates for multifunctional ultrathin piezoelectric devices.

In this work, based on first-principles calculations, we propose an altermagnetic semiconductor: Janus V_2AsBrO monolayer. It exhibits an out-of-plane magnetic easy axis and a Néel temperature (T_N) exceeding room temperature. Breaking the crystal symmetry through uniaxial strain induces significant valley splitting, demonstrating a robust piezovally effect. Furthermore, a strain-tunable piezomagnetic effect emerges under hole doping, generating a finite net M . Additionally, the monolayer exhibits a substantial out-of-plane piezoelectric coefficient (2.19 pm/V), as confirmed by theoretical calculations. The “multipiezo” effect combining piezovally, piezomagnetism, and piezoelectricity establishes the V_2AsBrO monolayer an exciting candidate for next-generation multifunctional devices in future nanoelectronics and spintronics.

II. METHODS

The first-principle calculations are performed using the projector augmented wave (PAW) method within density functional theory (DFT) [36, 37] as implemented in the plane wave code Vienna ab initio Simulation Package (VASP) [38–40]. The exchange-correlation functional employ the generalized gradient approximation (GGA) formulation of Perdew-Burke-Ernzerhof (PBE) [41]. The cut-off energy is set to 600 eV, and the convergence criteria for atomic force and energy are set to be 0.001 eV/Å and 10^{-7} eV, respectively. A Γ -centered Monkhorst-Pack grid of $12 \times 12 \times 1$ k-points is used to sample the Brillouin zone (BZ) of the unit cell. A vacuum layer of 20 Å is placed along the z direction to avoid interactions between adjacent layers. To deal with the strong correlation effect of the $3d$ orbitals of V atom, the GGA + U method ($U = 4.0$ eV) is employed for the V- $3d$ electron [23, 42, 43]. A $2 \times 2 \times 1$ supercell is adopted to calculate the phonon spectrum by using the PHONOPY code [44] based on the density functional perturbation theory (DFPT) [45]. The *ab initio* molecular dynamics (AIMD) simulations in the canonical (NVT) ensemble are performed for 3000 fs at 300 K with a Nosé-Hoover thermostat [46].

III. RESULTS AND DISCUSSION

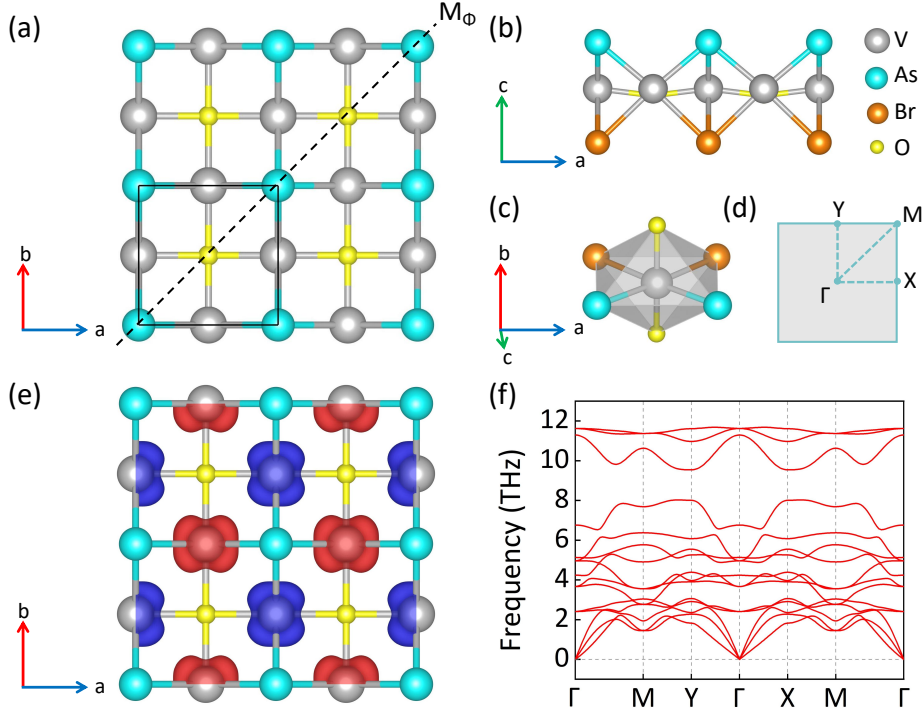


FIG. 1. (a) Top and (b) side views of the Janus V_2AsBrO monolayer. The unit cell is marked by the solid black line. M_Φ denotes a mirror operation performed along a diagonal direction in the ab plane. (c) Schematic diagram of V atoms in an octahedral crystal field for Janus V_2AsBrO monolayer. (d) The first Brillouin zone with high-symmetry points. (e) Top views of spin densities of the Janus V_2AsBrO monolayer. The spin-up density is shown in red and the spin-down density is shown in blue, respectively. (f) The phonon dispersion of the Janus V_2AsBrO monolayer.

Figure 1(a-b) illustrates the Janus V_2AsBrO monolayer crystal structure, characterized by diagonal mirror symmetry M_Φ . The monolayer adopts a tetragonal lattice (space group $P4mm$, No. 99), where a central V-O atomic layer is intercalated between As and Br termination layers. Each V atom is surrounded by two O, two As, and two Br atoms forming a highly distorted octahedral structure [Fig. 1(c)]. The Brillouin zone and high symmetry point of Janus V_2AsBrO monolayer are depicted in Fig. 1(d). Detailed structural information including lattice constants, bond lengths, and bond angles of Janus V_2AsBrO monolayer are summarized in Table S1 of the supplementary material [47]. To characterize the bonding nature of the Janus V_2AsBrO monolayer, we calculated its electron localization

function (ELF), as shown in Fig. S1 [47]. The ELF distribution reveals pronounced electron density accumulation around O, As, and Br atoms, indicating dominant ionic character in the V-O, V-As, and V-Br bonds. To identify the magnetic ground state, we evaluated four collinear spin configurations: ferromagnetic (FM) and three antiferromagnetic orderings (AFM1, AFM2, AFM3), see Fig. S2 [47]. Our calculations demonstrate that the AFM1 configuration exhibits the lowest total energy. The energy differences between competing magnetic orders and the AFM1 ground state are systematically tabulated in Table S2 [47].

The spin density of the Janus V_2AsBrO monolayer exhibits an anisotropic magnetization localized around the V atoms [Fig. 1(e)]. Notably, this spin density cannot be manipulated through inversion or translation symmetry, but instead requires a rotational operation, which is a distinguishing feature of altermagnets [48, 49]. Magnetic anisotropy, a fundamental property of magnetic materials, is essential for achieving long-range ferromagnetic ordering in 2D materials [42, 50]. Anisotropy is typically characterized by the magnetic anisotropy energy (MAE), which quantifies the energy variation with respect to the magnetization direction. The calculated MAE ($MAE = E_{[100]} - E_{[001]}$) is $110 \mu\text{eV}$ per unit cell, indicating a perpendicular magnetic anisotropy (PMA) character in the Janus V_2AsBrO monolayer. The strong PMA character is further demonstrated by the MAE distribution over the entire space, as shown in Fig. S3(a) [47]. Specifically, the MAE reaches its maximum value in the xy -plane and gradually decreases to zero as the magnetic axis rotates toward the z -direction. In addition, we calculated the T_N of the Janus V_2AsBrO monolayer to be 960 K [Fig. S3(b) [47]] using the Monte Carlo (MC) method based on the Heisenberg model. (More details can be found in the supplementary material.) The value of T_N is significantly higher than that of other altermagnets, such as Fe_2Se_2O (319 K) [34], Mn_2Se_2O (467 K) [51], and V_2Te_2O (740 K) [52].

To determine the stability of Janus V_2AsBrO monolayer, we performed first-principles calculations of phonon dispersion, AIMD simulations, and elastic tensor analysis. The phonon dispersion in Fig. 1(f) exhibits no imaginary frequencies throughout the entire Brillouin zone, confirming its dynamic stability. Furthermore, AIMD simulation at 300 K reveal minimal energy fluctuations ($\Delta E < [0.15] \text{ eV/atom}$) and preserved structural integrity over [3] ps trajectories (see Fig. S4 [47]), demonstrating robust thermal stability. The elastic constants ($C_{11} = 94.08 \text{ N/m}$, $C_{12} = 20.57 \text{ N/m}$, and $C_{66} = 34.65 \text{ N/m}$) of Janus V_2AsBrO monolayer satisfy the Born-Huang criteria for mechanical stability [53]: $C_{11} > 0$, $C_{66} > 0$,

$C_{11} > |C_{12}|$, confirming its mechanical stability. Besides stability, it is important to consider material strength and anisotropy for practical applications. Therefore, we calculated the angular-dependent elastic properties: Young's modulus $Y_{2D}(\theta)$ and Poisson's ratio $\nu_{2D}(\theta)$ (Fig. S5 [47]). The max (min) Young's modulus of Janus V_2AsBrO monolayer is 89.58 N/m (86.37 N/m). It is noteworthy that the Young's modulus of V_2AsBrO is lower than that of MoS_2 (124.5 N/m) [54], suggesting it can be easily tuned by strain. This makes the Janus V_2AsBrO monolayer highly suitable for novel flexible electronics and piezotronics applications. Besides, the max (min) Poisson's ratio of 0.24 (0.20) is almost equal to that in graphene (0.19) [55].

We systematically investigate the electronic properties of the Janus V_2AsBrO monolayer. As shown in Fig. 2(a), the spin-resolved band structure without SOC reveals a semiconductor character with a direct bandgap of 254.1 meV. The energy band structure shows the splitting of opposite spins in reciprocal space, confirming the characteristic feature of altermagnets. Mirror-symmetry-related valley degeneracy is identified at the Y and X high-symmetry points in both conduction and valence bands. Figure 2(b-c) presents the projected band structures for the V atoms demonstrating that the Y/X valleys in spin-up channels are dominated by d_{yz} orbitals, while d_{xz} orbitals primarily contribute to spin-down channels. Figure 2(d) shows the SOC-incorporated spin-resolved band structure, demonstrating preserved valley degeneracy.

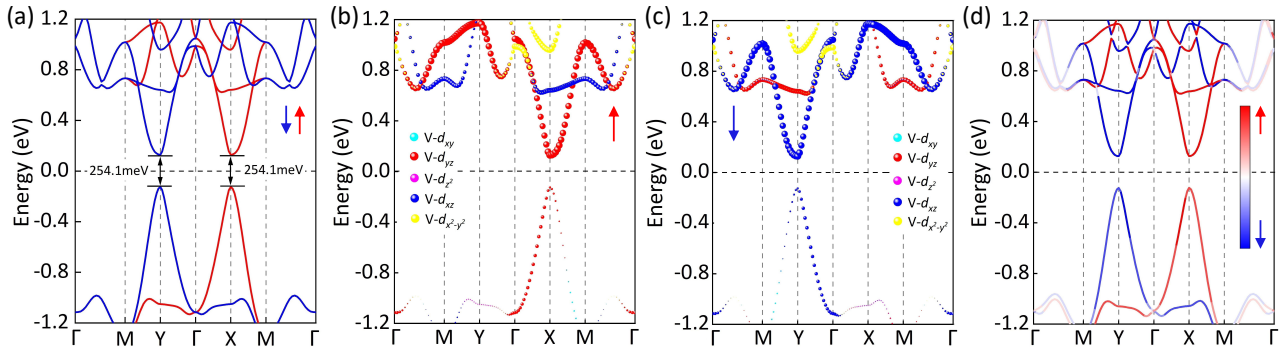


FIG. 2. (a) Spin-polarized electronic band structure of the Janus V_2AsBrO monolayer in the AFM ground state, calculated without SOC. (b, c) The V d -orbital-projected band structures for spin-up and spin-down channels (SOC excluded). (d) SOC-incorporated spin-resolved band structure, demonstrating preserved valley degeneracy.

Incorporating SOC effects [Fig. 2(d)], the valley degeneracy remains preserved, indicating that valley polarization in this altermagnet originates from spin splitting rather than SOC.

To further verify the SOC effect, we calculated the band structures with SOC under [100] and [010] magnetization directions (Fig. S6 [47]). While minor valley polarization ($\Delta E_v < [5]$ meV) emerges in these configurations, the negligible magnitude confirms the weak SOC-valley coupling. Consequently, SOC is excluded in subsequent calculations to isolate intrinsic altermagnetic effects.

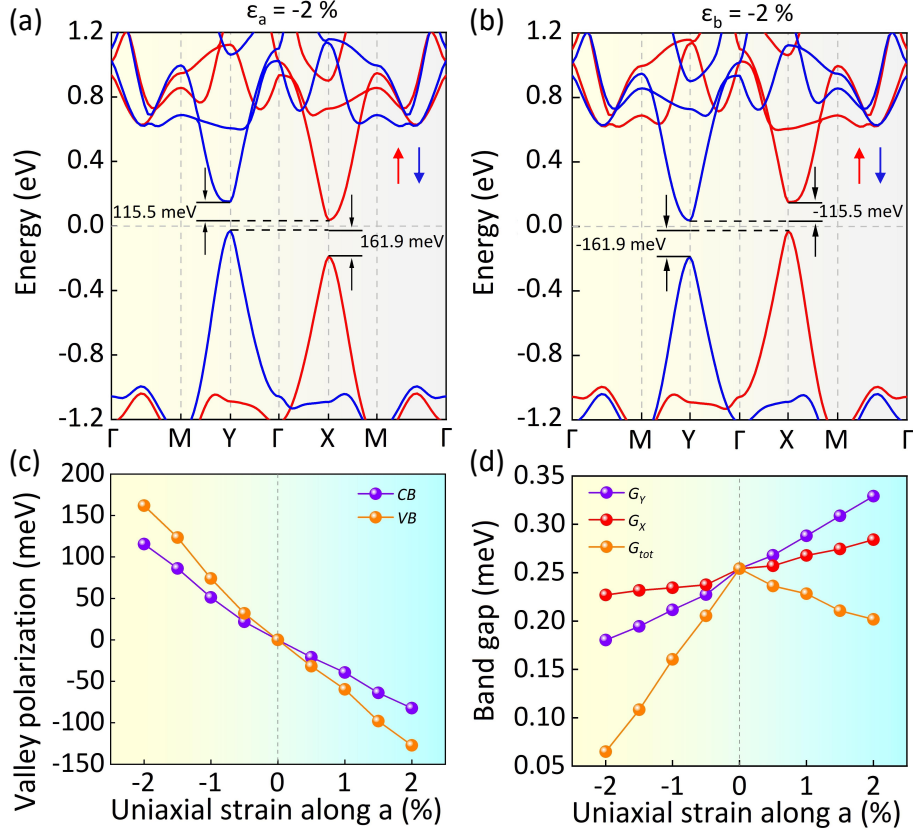


FIG. 3. Band structures of the Janus V_2AsBrO monolayer under -2% uniaxial compressive strain along (a) a direction and (b) b direction. (c) Strain-induced valley polarization in the conduction band (CB) and valence band (VB) under a direction uniaxial strain. (d) Evolution of valley gaps at Y and X [G_Y and G_X], as well as the total bandgap [G_{tot}] as function of a direction strain.

The piezovally effect manifests as a strain-mediated valley polarization mechanism, arising from the coupling between lattice deformation and spin-valley degrees of freedom in noncentrosymmetric crystals. Due to the M_Φ symmetry of the Janus V_2AsBrO monolayer, the two valleys at Y and X are degenerate. In the V_2AsBrO monolayer, the M_Φ symmetry enforces energy degeneracy between the Y and X valleys. Therefore, one can use in-plane

uniaxial strain along the a or b directions to break the crystal symmetry and induce substantial valley polarization. As shown in Figs. 3(a) and 3(b), the V_2AsBrO monolayer at -2% uniaxial strains along the a and b directions makes the energy of Y valley lower/higher than that of X valley. The value of valley polarization is 161.9 (155.5) meV at the valence band (conduction band) under 2% uniaxial strain along a direction [Fig. 3(a)], which is significantly larger than the reported values in 2D conventional ferrovalley materials requiring \mathcal{T} symmetry [56–59]. The Janus V_2AsBrO monolayer exhibits valley polarization of -161.9 (-155.5) meV at the valence band (conduction band) under -2% uniaxial strain along the b direction [Fig. 3(b)], indicating that the sign of valley polarization can be reversed by applying the uniaxial strain. As shown in Fig. 3(c), the valley polarization in the conduction band (CB) and valence band (VB) changes increase linearly under 0 to -2% and 0 to 2.0% uniaxial strains along the a direction, which can expands the scope of the study of valley materials. The energy difference (ΔE) and band structures of the V_2AsBrO monolayer under -2% to 2.0% uniaxial strain, which indicate that the Janus V_2AsBrO monolayer retains its altermagnetic properties, are presented in Fig. S7 ~ S9 [47]. In addition, Fig. 3(d) shows the variation in the overall band gap [G_{tot}] and the gaps of the Y and X valleys [G_Y and G_X]. It is clear that uniaxial strain promotes the separation of the Y and X valleys in both the conduction and valence bands from other bands, facilitating the experimental manipulation of these valleys. Furthermore, biaxial strain is also considered to adjust and control the electronic structure. The calculations indicate that the Janus V_2AsBrO monolayer retains its antiferromagnetic property, and the band gap gradually increases with the application of biaxial strain (see Figs. S10 and S11 [47]).

The physical mechanism underlying the piezomagnetic effect in the V_2AsBrO monolayer is illustrated in Fig. 4(a). Upon the manifestation of valley polarization in the band structure due to uniaxial strain, a net M emerges by precisely aligning the Fermi level to intersect a single valley through hole doping. The M is elucidated by the formula: $M = \int_{-\infty}^{E_F^{(n)}} [\rho^\uparrow(\varepsilon) - \rho^\downarrow(\varepsilon)] dE$, where E_F is the fermi level after doping, n is the doping density, and $\rho^\uparrow(\rho^\downarrow)$ is the spin-up (down) part of the density of states. Subsequently, an evaluation was conducted to determine the resultant magnetic moment M for distinct strains and varying hole doping levels. As shown in Fig. 4(b), under a certain hole doping concentration, the net M increases consistently with increasing uniaxial strain and eventually saturates. Notably, tensile and compressive strains induce opposite magnetic orientation. Analogously,

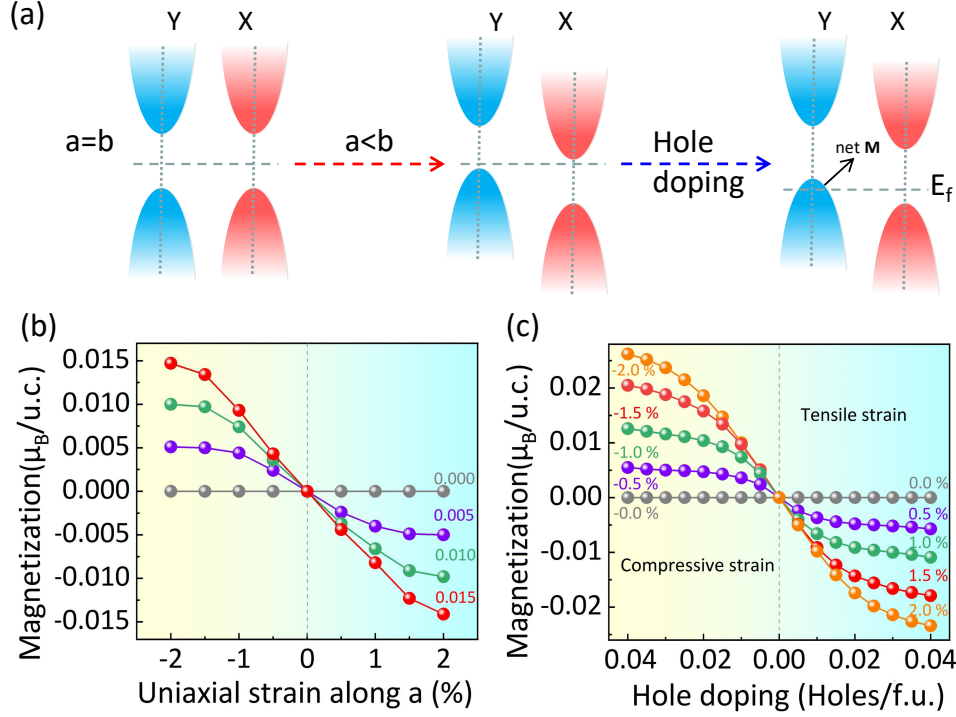


FIG. 4. (a) Schematic of the net magnetization (M) induced by hole doping in the Janus V_2AsBrO monolayer under certain uniaxial strain. (b) and (c) The corresponding net magnetization per unit cell for different concentrations of hole doping.

as shown in Fig. 4(c), for a certain uniaxial strain, the net M exhibits a gradual rise with increasing hole doping concentration, reaching a maximum saturation point with heightened doping levels. The band structures of V_2AsBrO monolayer subjected to uniaxial strain along the a direction, doped with 0.03 hole/f.u. are presented in Fig. S12 [47], thereby demonstrating the variation of net M polarization.

The piezoelectric effect is an intrinsic electromechanical coupling phenomenon in non-centrosymmetric materials. The application of strain or stress causes a charge redistribution, thereby leading to the formation of electric dipole moments and the production of electricity. Owing to the disruption of horizontal mirror symmetry, the Janus V_2AsBrO monolayer exhibits an out-of-plane piezoelectricity. The 2D manifestation of the piezoelectric effect is described by the piezoelectric stress coefficients (e_{ij}) and the piezoelectric strain coefficients (d_{ij}). The relaxed piezoelectric tensors (e_{ij} and d_{ij}) are obtained as the sum of electronic

and ionic contributions:

$$e_{ij} = \frac{\partial P_i}{\partial \varepsilon_j} = e_{ij}^{elc} + e_{ij}^{ion}, \quad (1)$$

$$d_{ij} = \frac{\partial P_i}{\partial \sigma_j} = d_{ij}^{elc} + d_{ij}^{ion}, \quad (2)$$

where the P_i , ε_j , and σ_j represent the piezoelectric polarizations, strains, and stresses, respectively. Using Voigt notation, the piezoelectric strain and piezoelectric stress tensors with C_{4v} point group can be expressed as:

$$\begin{pmatrix} 0 & 0 & 0 \\ 0 & 0 & 0 \\ e_{31} & e_{31} & 0 \end{pmatrix}, \quad (3)$$

$$\begin{pmatrix} 0 & 0 & 0 \\ 0 & 0 & 0 \\ d_{31} & d_{31} & 0 \end{pmatrix}. \quad (4)$$

The piezoelectric strain coefficients d_{ik} can be derived by piezoelectric stress coefficients e_{ik} and elastic stiffness coefficients C_{ik} :

$$e_{ik} = d_{ij} C_{jk}, \quad (5)$$

therefore, the out-of-plane piezoelectric coefficients d_{31} can be expressed as:

$$d_{31} = \frac{e_{31}}{C_{11} + C_{12}}. \quad (6)$$

The e_{31} of Janus V_2AsBrO monolayer can be directly calculated by using DFPT. The calculated e_{31} (2.52×10^{-10} C/m) mainly arises from the contribution of electrons, and the signs for the contributions of electrons (2.84×10^{-10} C/m) and ions (-0.32×10^{-10} C/m) in Janus V_2AsBrO monolayer is opposite. According to equations (6), the calculated d_{31} is 2.19 pm/V, which is significantly larger than that of the altermagnetic semiconductor Janus Cr_2SO monolayer ($|d_{31}| = 0.97$ pm/V) [60]. Notably, the d_{31} of Janus V_2AsBrO monolayer is over nine times greater than that of Janus V_2SeTeO monolayer (~ 0.24 pm/V) [23]. The large d_{31} provides the potential to tune the spin-split bands of the altermagnetic V_2AsBrO

monolayer via the piezoelectric effect, offering broad prospects for the development and design of novel piezoelectric devices. Furthermore, as shown in Fig. S13 [47], we calculated the planar averaged electrostatic potential energy variation along the z direction and the intrinsic polar field of the V_2AsBrO monolayer to reveal the origin of its piezoelectricity. The difference in electrostatic potential energy between the sides is 1.08 eV, which can be interpreted as a surface-dependent work function, indicating charge redistribution within the V_2AsBrO monolayer, as well as the existence of an out-of-plane dipole moment. The strength of the intrinsic polar field was deduced from the slope of the curve, approximately 0.37 eV/Å. The out-of-plane dipole and intrinsic polar field indicate internal polarization of the material, further suggesting the potential piezoelectricity of the Janus V_2AsBrO monolayer.

IV. CONCLUSION

In conclusion, we predict a 2D altermagnetic semiconductor Janus V_2AsBrO monolayer with a band gap of 254.1 meV based on first-principles calculations. The material exhibits excellent dynamic, thermal, and mechanical stability, as confirmed by phonon dispersion spectra, ab initio molecular dynamics simulations, and elastic constant analysis. Remarkably, the monolayer demonstrates a strong PMA character with the MAE of 110 μ eV per unit cell, and an ultrahigh T_N of 960 K derived from MC simulations, far exceeding room-temperature operational requirements. Uniaxial strain engineering in the V_2AsBrO monolayer induces sizeable valley splitting, revealing the piezovally effect. By further introducing hole doping under strain, a net magnetization can be generated, demonstrating a robust piezomagnetic effect. Additionally, the breaking of horizontal mirror symmetry results in a large out-of-plane piezoelectric coefficient $d_{31} = 2.19$ pm/V, which significantly exceeds those of other predicted 2D piezoelectric altermagnets. These multifunctional properties—altermagnetism, piezovally polarization, and piezoelectricity—are synergistically integrated into a single material, enabling unprecedented control over spin, valley, and mechanical degrees of freedom. Our findings highlight the Janus V_2AsBrO monolayer as a promising candidate for next-generation multifunctional devices in spintronics, valleytronics, and piezoelectric applications.

V. ACKNOWLEDGMENTS

This work was supported by the Natural Science Foundation of China under Grants (No. 22372142), the Innovation Capability Improvement Project of Hebei province (No. 22567605H), the Natural Science Foundation of Hebei Province of China (No. B2021203030), the Science and Technology Project of Hebei Education Department (No. JZX2023020). The numerical calculations in this paper have been done on the supercomputing system in the High Performance Computing Center of Yanshan University.

VI. REFERENCES

-
- [1] V. Baltz, A. Manchon, M. Tsoi, T. Moriyama, T. Ono, and Y. Tserkovnyak, Antiferromagnetic spintronics, [Rev. Mod. Phys.](#) **90**, 015005 (2018).
 - [2] J. Han, R. Cheng, L. Liu, H. Ohno, and S. Fukami, Coherent antiferromagnetic spintronics, [Nat. Mater.](#) **22**, 684 (2023).
 - [3] J. Wang, H. Zeng, W. Duan, and H. Huang, Intrinsic nonlinear Hall detection of the Néel vector for two-dimensional antiferromagnetic spintronics, [Phys. Rev. Lett.](#) **131**, 056401 (2023).
 - [4] S. Karube, T. Tanaka, D. Sugawara, N. Kadoguchi, M. Kohda, and J. Nitta, Observation of spin-splitter torque in collinear antiferromagnetic RuO₂, [Phys. Rev. Lett.](#) **129**, 137201 (2022).
 - [5] R. González-Hernández, L. Šmejkal, K. Výborný, Y. Yahagi, J. Sinova, T. Jungwirth, and J. Železný, Efficient electrical spin splitter based on nonrelativistic collinear antiferromagnetism, [Phys. Rev. Lett.](#) **126**, 127701 (2021).
 - [6] L. Šmejkal, R. González-Hernández, T. Jungwirth, and J. Sinova, Crystal time-reversal symmetry breaking and spontaneous Hall effect in collinear antiferromagnets, [Sci. Adv.](#) **6**, eaaz8809 (2020).
 - [7] L.-D. Yuan, Z. Wang, J.-W. Luo, E. I. Rashba, and A. Zunger, Giant momentum-dependent spin splitting in centrosymmetric low- Z antiferromagnets, [Phys. Rev. B](#) **102**, 014422 (2020).
 - [8] S. Hayami, Y. Yanagi, and H. Kusunose, Bottom-up design of spin-split and reshaped electronic band structures in antiferromagnets without spin-orbit coupling: Procedure on the

- basis of augmented multipoles, [Phys. Rev. B](#) **102**, 144441 (2020).
- [9] R. He, D. Wang, N. Luo, J. Zeng, K.-Q. Chen, and L.-M. Tang, Nonrelativistic spin-momentum coupling in antiferromagnetic twisted bilayers, [Phys. Rev. Lett.](#) **130**, 046401 (2023).
- [10] Y.-P. Zhu, X. Chen, X.-R. Liu, Y. Liu, P. Liu, H. Zha, G. Qu, C. Hong, J. Li, Z. Jiang et al., Observation of plaid-like spin splitting in a noncoplanar antiferromagnet, [Nature \(London\)](#) **626**, 523 (2024).
- [11] S. Reimers, L. Odenbreit, L. Šmejkal, V. N. Strocov, P. Constantinou, A. B. Hellenes, R. Jaeschke Ubierno, W. H. Campos, et al., Direct observation of antiferromagnetic band splitting in CrSb thin films, [Nat. Commun.](#) **15**, 2116 (2024).
- [12] D.-F. Shao, S.-H. Zhang, M. Li, C.-B. Eom, and E. Y. Tsymbal, Spin-neutral currents for spintronics, [Nat. Commun.](#) **12**, 7061 (2021).
- [13] L. Šmejkal, A. B. Hellenes, R. González-Hernández, J. Sinova, and T. Jungwirth, Giant and tunneling magnetoresistance in unconventional collinear antiferromagnets with nonrelativistic spin-momentum coupling, [Phys. Rev. X](#) **12**, 011028 (2022).
- [14] H. Bai, L. Han, X. Y. Feng, Y. J. Zhou, R. X. Su, Q. Wang, L. Y. Liao, W. X. Zhu, X. Z. Chen, F. Pan, X. L. Fan, and C. Song, Observation of spin splitting torque in a collinear antiferromagnet RuO₂, [Phys. Rev. Lett.](#) **128**, 197202 (2022).
- [15] M. Naka, S. Hayami, H. Kusunose, Y. Yanagi, Y. Motome, and H. Seo, Spin current generation in organic antiferromagnets, [Nat. Commun.](#) **10**, 4305 (2019).
- [16] Z. Feng, X. Zhou, L. Šmejkal, L. Wu, Z. Zhu, H. Guo, R. González-Hernández, X. Wang, H. Yan et al., An anomalous Hall effect in antiferromagnetic ruthenium dioxide, [Nat. Electron.](#) **5**, 735 (2022).
- [17] G. S. Diniz and E. Vernek, Suppressed Kondo screening in two-dimensional antiferromagnets, [Phys. Rev. B](#) **109**, 155127 (2024).
- [18] J. R. Schaibley, H. Yu, G. Clark, P. Rivera, J. S. Ross, K. L. Seyler, W. Yao, and X. Xu, Valleytronics in 2D materials, [Nat. Rev. Mater.](#) **1**, 16055 (2016).
- [19] G. Pacchioni, Valleytronics with a twist, [Nat. Rev. Mater.](#) **5**, 480 (2020).
- [20] S. A. Vitale, D. Nezich, J. O. Varghese, P. Kim, N. Gedik, P. Jarillo-Herrero, D. Xiao, and M. Rothschild, Valleytronics: Opportunities, challenges, and paths forward, [Small](#) **14**, 1801483 (2018).

- [21] S. Sattar, J. A. Larsson, C. M. Canali, S. Roche, and J. H. Garcia, Giant valley-polarized spin splittings in magnetized Janus Pt dichalcogenides, *Phys. Rev. B* **105**, L041402 (2022).
- [22] H.-Y. Ma, M. Hu, N. Li, J. Liu, W. Yao, J.-F. Jia, and J. Liu, Multifunctional antiferromagnetic materials with giant piezomagnetism and noncollinear spin current, *Nat. Commun.* **12**, 2846 (2021).
- [23] Y. Zhu, T. Chen, Y. Li, L. Qiao, X. Ma, C. Liu, T. Hu, H. Gao, and W. Ren, Multipiezo effect in altermagnetic V_2SeTeO monolayer, *Nano Lett.* **24**, 472 (2024).
- [24] W. Wu, L. Wang, Y. Li, F. Zhang, L. Lin, S. Niu, D. Chenet, X. Zhang, Y. Hao, T. F. Heinz, J. Hone, and Z. L. Wang, Piezoelectricity of single-atomic-layer MoS_2 for energy conversion and piezotronics, *Nature* **514**, 470 (2014).
- [25] M. Dai, Z. Wang, F. Wang, Y. Qiu, J. Zhang, C.-Y. Xu, T. Zhai, W. Cao, Y. Fu, D. Jia, Y. Zhou, and P.-A. Hu, Two-dimensional van der Waals materials with aligned in-plane polarization and large piezoelectric effect for self-powered piezoelectric sensors, *Nano Lett.* **19**, 5410 (2019).
- [26] Y. Guo, S. Zhou, Y. Z. Bai, J. J. Zhao, Enhanced piezoelectric effect in Janus group-III chalcogenide monolayers, *Appl. Phys. Lett.* **110**, 163102 (2017).
- [27] L. Wang, Z. Lin, Y. Du, J. Qiu, X. Chen, and J. Yu, The piezoelectricity of 2D Janus $ZnBrI$: Multiscale prediction, *Chem. Phys. Lett.* **794**, 139506 (2022).
- [28] Z. Wang, X. Yan, Y. Liu, and G. Yang, Piezoelectric response and ferromagnetic order in 2D Janus $FeGeN_3$, *Appl. Phys. Lett.* **124**, 122409 (2024).
- [29] Q. Ma, G. Yang, B. Wang, and Y. Liu, Large out-of-plane piezoelectric effect in a Janus ferromagnetic semiconductor monolayer of $CrOFBr$, *Phys. Rev. B* **110**, 064430 (2024).
- [30] Q. Ma, B. Wang, G. Yang, and Y. Liu, Emergent multifunctionality in the two-dimensional Janus $VSBrl$ monolayer: A study of multiferroicity, magnetoelectricity, and piezoelectricity, *Phys. Rev. B* **111**, 054104 (2025).
- [31] W. Wu and Z. L. Wang, Piezotronics and piezo-phototronics for adaptive electronics and optoelectronics, *Nat. Rev. Mater.* **1**, 16031 (2016).
- [32] C. Shi, J. J. Ma, J. Y. Jiang, M. M. Hua, Q. Xu, H. Yu, Y. Zhang, and H. Y. Ye, Large piezoelectric response in hybrid rare-earth double perovskite relaxor ferroelectrics, *J. Am. Chem. Soc.* **142**, 9634 (2020).

- [33] X. Chen, D. Wang, L. Y. Li and B. Sanyal, Giant spin-splitting and tunable spin-momentum locked transport in room temperature collinear antiferromagnetic semimetallic CrO monolayer, *Appl. Phys. Lett.* **123**, 022402 (2023).
- [34] Y. Wu, L. Deng, X. Yin, J. Tong, F. Tian and X. Zhang, Valley-related multipiezo effect and noncollinear spin current in an altermagnet Fe₂Se₂O monolayer, *Nano Lett.* **24**, 10534 (2024).
- [35] Q. Cui, B. Zeng, P. Cui, T. Yu, and H. Yang, Efficient spin seebeck and spin nernst effects of magnons in altermagnets, *Phys. Rev. B* **108**, L180401 (2023).
- [36] P. Hohenberg and W. Kohn, Inhomogeneous electron gas, *Phys. Rev.* **136**, B864 (1964).
- [37] W. Kohn and L. J. Sham, Self-consistent equations including exchange and correlation effects, *Phys. Rev.* **140**, A1133 (1965).
- [38] G. Kresse, Ab initio molecular dynamics for liquid metals, *J. Non-Cryst. Solids* **192-193**, 222 (1995).
- [39] G. Kresse and J. Furthmüller, Efficiency of ab-initio total energy calculations for metals and semiconductors using a plane-wave basis set, *Comput. Mater. Sci.* **6**, 15 (1996).
- [40] G. Kresse and D. Joubert, From ultrasoft pseudopotentials to the projector augmented-wave method, *Phys. Rev. B* **59**, 1758 (1999).
- [41] J. P. Perdew, K. Burke, and M. Ernzerhof, Generalized gradient approximation made simple, *Phys. Rev. Lett.* **77**, 3865 (1996).
- [42] X. Cheng, S. Xu, F. Jia, G. Zhao, M. Hu, W. Wu, and W. Ren, Intrinsic ferromagnetism with high Curie temperature and strong anisotropy in a ferroelastic VX monolayer (X = P, As), *Phys. Rev. B* **104**, 104417 (2021).
- [43] J.-Y. Li, A.-D. Fan, Y.-K. Wang, Y. Zhang, and S. Li, Strain-induced valley polarization, topological states, and piezomagnetism in two-dimensional altermagnetic V₂Te₂O, V₂STeO, V₂SSeO, and V₂S₂O, *Appl. Phys. Lett.* **125**, 222404 (2024).
- [44] A. Togo and I. Tanaka, First principles phonon calculations in materials science, *Scripta. Mater.* **108**, 1 (2015).
- [45] X. Gonze and C. Lee, Dynamical matrices, Born effective charges, dielectric permittivity tensors, and interatomic force constants from density-functional perturbation theory, *Phys. Rev. B* **55**, 10355 (1997).
- [46] G. J. Martyna, M. L. Klein, and M. Tuckerman, Nosé-Hoover chains: The canonical ensemble via continuous dynamics, *J. Chem. Phys.* **97**, 2635 (1992).

- [47] See the Supplemental Material at <https://link.aps.org/supplemental/10.1103/PhysRevB.xx.xxxxxx> for ELF plot, structural parameters, different magnetic configurations, energy difference between different magnetic orders and the AFM1 order, details on the Curie temperature simulations, the 3D MAE as well as the temperature-dependent magnetic moments and magnetic susceptibility, total energy fluctuations during AIMD simulations, Young's modulus and Poisson's ratio, band structures under SOC with [100] and [010] magnetization, energy difference (ΔE) and band structures under uniaxial and biaxial strain (-2% to 2%), band structures with the hole doping concentration under uniaxial strain along the a direction from -2% to 2% , and planar average electrostatic potential energy of the Janus V_2AsBrO monolayer.
- [48] L. Šmejkal, J. Sinova, and T. Jungwirth, Emerging research landscape of altermagnetism, *Phys. Rev. X* **12**, 040501 (2022).
- [49] L. Šmejkal, J. Sinova, and T. Jungwirth, Beyond conventional ferromagnetism and antiferromagnetism: A phase with nonrelativistic spin and crystal rotation symmetry, *Phys. Rev. X* **12**, 031042 (2022).
- [50] A.-N. Ma, P.-J. Wang, and C.-W. Zhang, Intrinsic ferromagnetism with high temperature, strong anisotropy and controllable magnetization in the CrX ($X = P, As$) monolayer, *Nanoscale* **12**, 5464 (2020).
- [51] F.-F. Huang, P. Jiang, X. Zheng, H.-M. Huang, and Y.-L. Li, Emerging two-dimensional half-metal with high Curie temperature and strain-tunable altermagnetism, *Phys. Rev. B* **110**, 174429 (2024).
- [52] Q. Cui, Y. Zhu, X. Yao, P. Cui, and H. Yang, Giant spin-Hall and tunneling magnetoresistance effects based on a two-dimensional nonrelativistic antiferromagnetic metal, *Phys. Rev. B* **108**, 024410 (2023).
- [53] R. C. Andrew, R. E. Mapasha, A. M. Ukpong, and N. Chetty, Mechanical properties of graphene and boronitrene, *Phys. Rev. B* **85**, 125428 (2012).
- [54] D. Çakır, F. M. Peeters, and C. Sevik, Mechanical and thermal properties of h -MX₂ ($M = Cr, Mo, W$; $X = O, S, Se, Te$) monolayers: A comparative study, *Appl. Phys. Lett.* **104**, 203110 (2014).
- [55] A. Politano, A. R. Marino, D. Campi, D. Farías, R. Miranda, and G. Chiarello, Elastic properties of a macroscopic graphene sample from phonon dispersion measurements, *Carbon* **50**, 4903 (2012).

- [56] C. Zhang, Y. Nie, S. Sanvito, and A. Du, First-principles prediction of a room-temperature ferromagnetic Janus VSSe monolayer with piezoelectricity, ferroelasticity, and large valley polarization, [Nano Lett.](#) **19**, 1366 (2019).
- [57] P. Jiang, L. Kang, Y.-L. Li, X. Zheng, Z. Zeng, and S. Sanvito, Prediction of the two-dimensional Janus ferrovalley material LaBrI, [Phys. Rev. B](#) **104**, 035430 (2021).
- [58] P. Zhao, Y. Dai, H. Wang, B. Huang, and Y. Ma, Intrinsic valley polarization and anomalous valley hall effect in single-layer 2H-FeCl₂, [ChemPhysMater.](#) **1**, 56 (2022).
- [59] B. Huang, W.-Y. Liu, X.-C. Wu, S.-Z. Li, H. Li, Z. Yang, and W.-B. Zhang, Large spontaneous valley polarization and high magnetic transition temperature in stable two-dimensional ferrovalley YX₂ (X = I, Br, and Cl), [Phys. Rev. B](#) **107**, 045423 (2023).
- [60] S.-D. Guo, X.-S. Guo, K. Cheng, K. Wang, and Y. S. Ang, Piezoelectric altermagnetism and spin-valley polarization in Janus monolayer Cr₂SO, [Appl. Phys. Lett.](#) **123**, 082401 (2023).